REPORT DOCUMENTATION PAGE

Form Approved
OMB No. 0704-0188

1. AGENCY USE ONLY (*Leave Blank*)	2. REPORT DATE	3. REPORT TYPE AND DATES COVERED
	30 APRIL 1997	FINAL - 1 AUG 1996 - 31 JAN 1997

4. TITLE AND SUBTITLE

FOCUSED APPLICATION SOFTWARE FOR DESIGN OF FERRITE PATCH ANTENNAS (SBIR - PHASE I)

5. FUNDING NUMBERS

PR
F49620-96-C-0030

6. AUTHOR(S)

BRIAN ANDERSON AND JOHN SILVESTRO

7. PERFORMING ORGANIZATION NAME(S) AND ADDRESS(ES)

ANSOFT CORPORATION
FOUR STATION SQUARE, SUITE 660
PITTSBURGH PA 15219

8. PERFORMING ORGANIZATION

AFOSR-TR-97
0190

9. SPONSORING/MONITORING AGENCY NAME(S) AND ADDRESS(ES)

USAF, AFMC
AIR FORCE OFFICE OF SCIENTIFIC RESEARCH
110 DUNCAN AVENUE SUITE B115
BOLLING AFB DC 20332-8080

nm

10. SPONSORING/MONITORING AGENCY REPORT NUMBER

11. SUPPLEMENTARY NOTES

12a. DISTRIBUTION/AVAILABILITY STATEMENT

Unlimited

12b. DISTRIBUTION CODE

DTIC QUALITY INSPECTED 2

DISTRIBUTION STATEMENT A
Approved for public release;
Distribution Unlimited

13. ABSTRACT (*Maximum 200 words*)

Currently, most antenna array designs are mechanically steered. However, as demand for higher performance antennas increases, an electronic replacement for the mechanical system becomes necessary. An altermative that may prove to be more cost effective is to use ferrite patch antennas as the elements in the array. The antenna's radiation characteristics are controlled by the direction and magnitude of the imposed magnetic fields that bias the ferrite. This is accomplished without requiring additional circuitry in the signal path. An initial study of this type of device was performed. The advanced ferrite handling capability of Ansoft HFSS was used to simulate the radiation characteristics of ferrite patch antennas. The simulation capability of this finite element field simulation tool with its advanced absorbing boundary condition to simulate ferrite patch antennas was studied. The advantage of this type of solver is the ability to analyze ferrites with non-uniform bias fields. Through this investigation a better understanding of the operating characteristics of ferrite patch antennas was achieved.

14. SUBJECT TERMS	15. NUMBER OF PAGES
FERRITE PATCH ANTENNAS, ANTENNA ARRAYS, FINITE ELEMENT METHOD	30
	16. PRICE CODE

17. SECURITY CLASSIFICATION OF REPORT	18. SECURITY CLASSIFICATION OF THIS PAGE	19. SECURITY CLASSIFICATION OF ABSTRACT	20. LIMITATION OF ABSTRACT
UNCLASSIFIED	UNCLASSIFIED	UNCLASSIFIED	UNCLASSIFIED

Chapter 1 Introduction

During this project we investigated the use of a finite element based field simulation tool for studying the radiation from patch antennas that have ferrite substrate or superstrates. We used a beta copy of an existing solver and made the appropriate changes to accommodate current sources. This solver is the one in Ansoft's HFSS (the tool that was formally known as Ansoft's Maxwell Eminence). The goal of this project was to determine if it would be possible to steer the beam in a ferrite patch antenna simply by changing the biasing field of the ferrite, and to determine if a finite element method (FEM) solver could be used to design such a device.

We discovered that a biased ferrite sub/superstrate radiating device often has a large surface or volume waves the can seriously affect its performance. We found this to be true when trying to compare our data with that found using other analysis techniques. We found that comparisons of our FEM simulations with those computed by a solver that assumes an infinite substrate were marginal for some cases. After further investigation of these geometries we found that there were sizable surface and/or volume waves present that made such comparisons difficult. We were successful in analyzing the radiation from a finite sized ferrite patch antenna that was used to generate a circularly polarized wave, and were able to shown beam steering in a finite sized patch antenna that was similar to one from the literature. In the latter two cases the data presented in the literature was measured. We also looked at the effect of bias field strength and bias field uniformity on the beam steering.

In conclusion we found that large surface and/or volume waves can affect the radiation from ferrite patch antennas and so call into question some of the available analysis techniques that assume an infinite planar sub/superstrate.

Chapter 2 Microwave Ferrites and Implementation in Ansoft HFSS

The three-dimensional full-wave finite element field simulator Ansoft HFSS version 5 includes gyrotropic ferrite materials. When losses are neglected, ferrite materials are described by an Hermitian permeability tensor[1]. Prior to version 5 of HFSS only anisotropic materials represented by a diagonal form via rotation of the coordinate system could be analyzed. Gyrotropic tensors could not be analyzed. Incorporating the ferrite material type required extensive changes to the entire finite element solution procedure. The foundation of these changes and their effects were originally described in [2][3], but a synopsis of the changes in the solution procedure will be presented in this chapter.

Section 2.1 Gyrotropic Ferrite Materials

Gyrotropic ferrite materials under small signal conditions are characterized by an Hermitian permeability tensor of the form[4]:

$$\bar{\bar{\mu}} = \mu_o \begin{bmatrix} 1+\chi & -j\kappa & 0 \\ j\kappa & 1+\chi & 0 \\ 0 & 0 & 1 \end{bmatrix} \tag{1}$$

where:

$$\chi = \frac{\omega_o \omega_m}{\omega_o^2 - \omega^2} \tag{2}$$

$$\kappa = \frac{\omega \omega_m}{\omega_o^2 - \omega^2} \tag{3}$$

and the uncoupled z direction is determined by the direction of the magnetostatic bias fields within the ferrite materials.

Equations 2 and 3 give the tensor components in terms of intermediate values which are functions of the ferrite material's properties, the operating frequency and the net internal bias field. The intermediate terms' dependence on these quantities are given as follows:

$$\omega = 2\pi f \tag{4}$$

$$\omega_o = -\gamma \mu_o H_o \tag{5}$$

$$\omega_m = -\gamma \mu_o M_s \tag{6}$$

where:

γ - material parameter indicating the origin of the material's magnetic moments; spin, orbital or both

H_o - the net internal bias field within the ferrite

M_s - the saturation magnetization of the ferrite

To add magnetic losses, the term ω_o can be replaced by $\omega_o + j\omega\alpha$, where:

$$\alpha = \frac{-\Delta H \gamma \mu_o}{2\omega} \tag{7}$$

and ΔH is the measured ferromagnetic line width of the ferrite material. The inclusion of magnetic losses in the permeability tensor removes the Hermitian (conjugate) symmetry and results in a complex unsymmetric tensor. This has an impact on the

methods used to solve the resulting finite element matrix equations. These modifications will be discussed later.

While the permeabiliy tensor's dispersion makes the analysis of ferrite loaded devices difficult, the greatest hurdle is often presented by the dependence on the externally applied magnetostatic bias fields. The magnetostatic fields in any non-ellipsoidal ferrite sample are not uniform, resulting in a spatially inhomogeneous permeability tensor. Spatially inhomogeneous bias fields have two affects on the tensor. First, the net internal field in equation (5) will vary throughout the tensor, resulting in tensor components that vary spatially. Second, variations of the direction of the static magnetization field will rotate the uncoupled z axis of the tensor into alignment with the bias field direction. This implies that the high-frequency field components which are coupled by the off diagonal terms in the tensor will vary throughout the sample. Accounting for the combination of varying tensor component magnitudes and tensor coordinate systems virtually eliminates analytic methods from accurate simulation of ferrite devices[5][6].

Section 2.2 Wave Propagation in Ferrites

As with other types of anisotropic materials, wave propagation in ferrites can occur in a variety of manners[7]. Some are analogous to the modes of propagation in isotropic dielectric materials. In other applications, Faraday rotation can occur. Further complicating the analysis of finite sized devices is the ease with which ferrites can support surface waves. Experimental thin-film devices have been fabricated which exploit the ferrite's capability of supporting different types of surface waves. Unfortunately, surface waves can readily occur in instances where they are not intended.

Section 2.3 Finite Element Analysis of Ferrite Loaded Devices

Finite element analysis is particularly well suited to the simulation of devices containing spatially inhomogeneous materials since the method allows the material properties to be different within each finite element. This capability was exploited in the Ansoft HFSS version 5 implementation with some basic assumptions, which will be detailed in this section.

Ansoft HFSS solves the vector wave equation for the electric field, $\overline{E}$,

$$\nabla x \overline{\overline{\mu}}^{-1} \nabla x \overline{E} - k_o^2 \varepsilon_r \overline{E} = 0 \tag{8}$$

The wave equation form shown here is modified to include the tensor permeability. Applying Galerkin's method, a form of the wave equation can be arrived at which is appropriate for the finite element solution technique:

$$\iiint_V \overline{W} \bullet \left[\nabla x \overline{\overline{\mu}}^{-1} \nabla x \overline{E} - k_o^2 \varepsilon_r \overline{E} \right] dV = 0 \tag{9}$$

which can be reduced to a form that does not require second order approximation functions by applying a vector identity and the divergence theorem. This results in the form:

$$\iiint_V \left[\left(\nabla x \overline{W} \right) \bullet \overline{\overline{\mu}}^{-1} \left(\nabla x \overline{E} \right) - k_o^2 \varepsilon_r \overline{W} \bullet \overline{E} \right] dV + \oiint_A \left[\overline{W} x \left(\nabla x \overline{E} \right) \right] \bullet d\overline{a} = 0 \tag{10}$$

The additional surface term can include many types of boundary conditions, from the most common Neumann and Dirichlet (magnetic and electric walls, respectively) to absorbing boundary conditions. The surface term also provides the entry point for source terms in the matrix equation. In HFSS, the source terms are most commonly ports but can include voltage and current gap sources.

Applying the finite element procedure to the Galerkin form (10) results in a sparse matrix equation that can be solved with well known matrix solution routines. The resultant matrix that is solved has the form

$$Ax = b \tag{11}$$

Where the elements of A result from a discretization of (10) over the individual finite elements and a precomputation of the simple integrals over the finite element. Specifically the elements of A have the form:

$$A_\Omega = \iiint_\Omega \left[(\nabla x \overline{w}) \bullet \overline{\overline{\mu}}^{-1} (\nabla x \overline{w}) - k_o^2 \varepsilon_r \overline{w} \bullet \overline{w} \right] d\Omega \tag{12}$$

where:

$\overline{w}$ is the vector of finite element basis functions[8][9]. Vector finite elements are used for this basis in Ansoft HFSS. These basis have distinct advantages over traditional nodal based finite elements for electromagnetic wave propagation problems. Most importantly they avoid the occurrence of spurious mode but they also provide a natural enforcement of Maxwell boundary conditions at inter-element interfaces.

Ω is the domain of the finite element, which are tetrahedra in the case of HFSS.

The basis functions are represented in barycentric coordinates, which allow the integrals to be computed independent of the tetrahedra coordinates. This makes computation of the local terms of the finite element matrix a simple matter of substituting the tetrahedral coordinates into the pre-computed integrals for a general tetrahedra.

The driving vector b is a finite element discretization of the source terms, whether they result from ports or voltage/current gap sources, along the surface of the source.

For lossless isotropic dielectrics the components of matrix A are all real and the matrix is symmetric allowing a sparse, symmetric real matrix solver to be applied. Symmetry allows the solution procedure to store and work on half of the problem, thereby reducing the memory requirements at solve time. If the dielectrics have loss, a complex form of the matrix solver can be used. The complex matrix solver uses twice the memory of the real solver due to the increased size of the complex data type. Both of the matrix solvers have existed in HFSS for many years.

In the case of ferrites, the lossless case forces the matrix A to be represented as an Hermitian matrix and the complex matrix solver has been modified to assume conjugate symmetry during the solution process. No additional memory is required to solve an Hermitian matrix versus the complex symmetric solver. When loss is included in ferrite problems, either magnetic loss from the ferrite or dielectric losses from any object in the solution, a complex unsymmetric matrix solver must be used. In this case the solver requires twice the memory of the complex symmetric and solution times also increase by a factor of two.

Instances where the device's s-parameters are desired, (11) can be formulated via the transfinite element procedure [10] in such a way that they occupy a portion of the solution vector x. Thereby the s-parameters are a variationally stable quantity of the formulation and achieve accurate convergence sooner than the corresponding electromagnetic fields.

Section 2.4 High-Frequency Calculations including Non-uniform Magnetostatic Fields

Analyzing a ferrite loaded device including the effects of non-uniform magnetostatic fields and the resulting spatially inhomogeneous permeability tensor can be divided into two parts. First, the magnetostatic fields must be solved. Then these fields are used to fill in the permeability tensor on a finite element by finite element basis. Either approximate analytic techniques or numerical methods can be employed to find the

magnetostatic fields. In HFSS we have used Ansoft's previously existing non-linear magnetostatic field solver, Maxwell® 3D Field Simulator (M3DFS).

Prior to solving for the magnetostatic fields, the coordination of the M3DFS and HFSS projects must be made. First, the two projects must share objects which are necessary to each solution. Typically the objects which fall into this category are the ferrite materials which are characterized by the tensor permeability in HFSS and a non-linear B-H curve in M3DFS. Other objects such as non-magnetic dielectrics or conductors are not included in the static M3DFS analysis. Likewise, magnets may be included in the high-frequency HFSS analysis as boundary conditions without requiring the solution of the rf fields throughout the object. Additionally, any objects outside the high-frequency ground structure need not be included in the HFSS model. During the model definition phase, care must be taken to ensure that the shared ferrite objects lie at the same location in both projects, since HFSS will look at specific points for the magnetostatic fields.

As stated above, ferrite materials are characterized by a non-linear B-H curve in the static M3DFS analysis. In some instances these curves are provided by the ferrite manufacturer, but in many instances an approximate curve is all that is available. In either case, the saturation point where the B-H curve transitions from the large initial permeability slope to the slope of free space is the value of the saturation magnetization used in the tensor permeability (6). Once the non-linear characteristics of the ferrite are modeled, any other magnetic objects are added to the project. These can include: permanent magnets, electromagnets, magnetic spacers and magnetic yokes. From this project definition, the solution proceeds adaptively until a user specified error limit is reached.

Once the magnetostatic fields are computed, the high-frequency analysis can proceed. During the problem definition phase, the user selects that non-uniform bias fields are to be used and then specifies the name of the magnetostatic project. While HFSS is adaptively solving the high-frequency project, it interrogates the magnetostatic project for the fields at the centurions of its tetrahedra which lie in ferrite materials. Within each tetrahedra, the tensor permeability is assumed to be uniform. While this is

not necessarily the case, the refinement procedure will reduce the tetrahedral size in regions where the high-frequency fields require greater mesh density. As the finite element size is reduced, the uniform fields within each element will become better.

Chapter 3 Results

Section 3.0 Introduction

From our study of ferrite patch antennas we have found that FEM based simulations do a reasonable, and in the case of a circularly polarized antenna an excellent job of simulating antennas on a finite sized ferrite. We have also found that when such simulations do not compare well when compared to data from the literature that assumes a ferrite substrate of infinite extent. For the infinite ferrite data available in the literature we will show how surface and/or volume waves present in such geoemtries make it difficult for an FEM based simulation to repeat such data.

Before presenting the results a few comments on how Ansoft's HFSS computes the quantities presented here. The software allows the user to view the fields both inside and outside of the solution region. One of the options is to view shade plots of the magnitude of the steady state electric field inside the solution space at a series of time steps. The quantity plotted is: $|\text{Real}\{\mathbf{E}\, e^{j\omega t}\}|$, for a series of $j\omega t$ phase angles. To study the fields outside of the solution space the solver has an option for computing the radiated fields for problems where the solution space is bounded by an advanced second order absorbing boundary condition [11]. The software uses the fields on the ABC to compute the far zone fields using the equivalence principle (for more details see [11]). Therefore whatever fields are present on the ABC will contribute to the patterns. Note, based on our experience we have found that by placing the ABC $\lambda/4$ from the radiating device that it provides satisfactory results. For the cases presented here the ABC was placed $\lambda/4$ or more from the patch.

Section 3.1 Comparisons with Other Solution Techniques

As was stated in our original proposal, there exist several papers in the literature that a deal with the simulation of ferrite patch antennas. To summarize the relevant ones we can start by considering the original work by Pozar. In reference 15 he considered the

radiation and scattering from microstrip patch antennas on an infinite planar ferrite that was biased normal to the substrate. The method of moments (MOM) was used to compute the resonant frequency and the radiation characteristics. He was mostly interested in the ability of a ferrite patch antenna to generate a circularly polarized field using only a single feed point. In a separate effort, Hsia et al have also been working on a computational model of a ferrite patch antenna. This work is summarized in Reference 12, where the radiation from a current element on a grounded sub/super-strate geometry is considered. In this case the substrate is assumed to be isotropic and the superstrate is a biased ferrite. By studying the radiation from this geometry one can determine the general radiation characteristics of a microstrip patch antenna with the same substrate/superstrate combination. Here again the substrate and superstrate are assumed to be infinite planar geometries. One of the drawbacks of an MOM simulation such as the one mentioned above is that the Green's function for determining the electric field from a current element must be known in advance. This limits the MOM to only certain classes of problems, and for microstrip (with or without ferrites) the dielectric layer must be infinite in extent when considering radiation problems. While this limitation causes no problems for standard microstrip geometries [13], it does appear that it may be problematic for biased ferrite substrates.

Consider the data shown in Figure 3.1. In this case we see a comparison of our computed results with those from Reference 12. It shows the radiation from an ideal current dipole on an isotropic substrate ($\varepsilon r = 12.9$) with a biased ferrite as a superstrate. The ferrite has an $\varepsilon_r = 15.1$, $\mu_0 M_0 = 0.16T$, the biasing field is x directed and $w_0/w_m = 0.7$ for this case. The current element is x directed and sits on top of the ferrite. The geometry analyzed using HFSS, with dimensions, is shown in Figure 3.2. Note the finite size of the solution space required for an FEM simulation such as this. The dielectric in this model extends right to the absorbing boundary. For this case the $E\phi$ fields on the phi=90 deg cut plane was computed and the results shown reasonable agreement. In Reference 12 it was shown that by varying the bias field value the radiation pattern in this cut plane could be scanned in angle. Consider next the data shown in Figure 3.3 is the same field values, but for the case where $\omega_0/\omega_m = 0.3$. For this case the data from [12] shows that the main beam

should be scanned to an angle of approximately 60 deg. There is some change in the radiation from that shown in Figure 3.1, but as one can see not the same dramatic change as was reported in [12]. We believe that it is due to the finite size of our simulation. To test this hypothesis we next looked at the electric fields inside the FEM solution space. Figures 3.4, show shade plots of the magnitude of the electric field on a cut plane that is on the x-y plane (see Figure 3.2). The field plotted here is the steady state electric field at a series of phase angles. As we can see from this time progression there is a sizable surface wave that is excited at the substrate-superstrate interface. This wave propagates along the ferrite surface until it is absorbed at the solution space boundary, the ABC. Since the data from Reference 12 assumes the two layers are infinite in extent we believe that we effectly solving two different problems. A important point to make at this point is that the radiated fields computed here are determined using the equivalence principle and the values of the fields on the ABC. Therefore any surface waves present on this boundary affect the radiated fields, as would be the case in a real world device where a finite ferrite substrate is used. We know from our earlier work that the FEM analysis used here works quite well for analyzing circulators. With circulators though, the ferrite is of a finite size. We believe that the discrepancies we saw in trying to compare to MOM analyses such as in [15] or the data such as presented here is due to the infinite substrate assumption. In fact we wonder if this surface wave might have a lot to do with the beam steering that is reported in such analyses. By varying the bias the effective permittivity of the ferrite is changed [14] and as such we believe the propagation constant of the surface wave. This variation in the propagation constant and we assume the surface and or volume waves radiation characteristics may be a major part of the beam steering seen in the previous work. This would be an interesting idea for future research, but it is beyond the scope of this study. To verify that the surface wave may be affecting the radiation characteristics a slightly different model of this problem was also solved. The geometry is shown in Figure 3.5. The current element and bias fields for this case are the same as was used to generate the data presented in Figure 3.1, except the substrate and superstrate do not extend to the ABC. Instead a small layer with the same thickness as the combined substrate-superstrate was added around the antenna. This new layer has an ε_r=15.1, but

with a loss tangent of 0.4. The effect of this small layer is to act as an artificial absorber that reduces the magnitude of the surface wave . By viewing the steady state field values in the solution space for a variety of phase angles it can be seen that this absorber reduced the size of the surface wave that eventually impinges on the ABC. It did not eliminate it though. Figure 3.6 shows a comparison of the radiation patterns for this new geometry when compared to the data from Figure 3.1. As we can see, by reducing the surface wave somewhat it did effect the radiation. This has caused us some concern as much of the analysis in the literature assumed infinite substrates and it appears that for this class of problems where large surface and or volume waves are present that may not be a valid model for a real world device.

The data presented in Reference 15 was more concerned with the circularly polarized nature of a ferrite patch antenna. We have a better test case for considering that effect that will be presented in the next section. It should also be noted that in this paper, data for the radiation from an infinite array of patch antennas in a phased array was also studied. The reflection coefficient of a single element in such an array is presented. We are almost at the stage in our product development where a set of matching boundaries can be used to analyze such phased array geometries. Once we have that feature completed this would make an excellent test case to verify the statements made in this section since the matching boundary simulation effectively simulates the fields in a single element when it is in an infinite array. Any surface wave effects should be modeled correctly in such an analysis. Therefore if good agreed is found between such a simulation and the data from [15] that would tend to reinforce the conclusions presented here. Here again that is beyond the scope of this project.

Section 3.2 Patch Antennas on a Finite Substrate

After coming to the conclusion that surface and/or volume wave effects would make direct comparisons with the data from the literature difficult to perform, we set about trying to find test cases where finite substrates were used. This meant that we would have to find measured results. We did in fact find 2 examples of such an analysis, the only problem is that since this is such a new area of application for ferrites (as

compared to circulators) the information contained in these papers is incomplete, especially with regard to the ferrite characteristics. Therefore for the cases presented in this section we had to make some educated guesses about certain details of the antenna under consideration. The first of the 2 works is the pioneering work of James et al [16]. This is the landmark paper that first showed that by biasing a ferrite one could steer the beam and as such opened up the possibility of using the DC bias field to steer an array of patch antennas. The second is a very recent paper by Sekhar et al [17]. This latter paper describes an experimental study of a circular patch antenna that was used to create a circularly polarized signal with a single feed point using a biased ferrite for the substrate.

Lets first consider the work of James et al [16]. The antenna in this case is not completely described in the paper. The model that was analyzed is shown in Figure 3.7. Again a ferrite superstrate is on top of an isotropic substrate ($\varepsilon_r = 10$). The patch is a circular antenna that resides on the interface between the two dielectrics. The antenna is fed by a coax from below. The paper does not give details of the feed (feed point and coax dimensions), and there is some confusion regarding the dielectric sizes: widths, lengths and thickness. Also details of the ferrite used are incomplete. We decided though that by setting up a similar problem we should at least be able to show similar beam steering as was found here. It may not be exact, but we should be able to replicate the steering seen in the paper. The dimensions of the geometry we solved is shown in Figure 3.7. The ferrite values we used are: $4\pi M_s$ =2500G, ΔH=500Oe, $\varepsilon_r = 13.8$ and the biasing field is y directed. We used a standard SMA coax for the feed and guessed at a feed location. Figure 3.8 shows the magnitude of the far zone electric field for the case of the bias field equal to zero and for the case where the bias field was 200 Oe. The data is for the $\phi = 0$ deg. plane. For this cut and this field component the measured data presented in Reference 16 showed a beam steer of 15 degs. As we can see there is a steering of the beam when the bias is applied for the case shown in Figure 3.8. For this case it is approximately 30 deg. While we had more of a steer and our main beam is somewhat broader than the one shown in [16], we think this does show the possibility of using bias fields to steer a beam.

We next used this model to test the performance of this antenna under a few different bias arrangements. Figure 3.9 shows the pattern data for the same geometry and field orientation as described in Figure 3.7, but with the internal bias field set to 300 Oe. As we can see there is very little change in the pattern when compared to the 200 Oe data. For small changes in bias field strength the antennas radiation characteristics do not appear to change significantly. Next we considered the effect of a non-uniform bias field. To accomplish this we split the ferrite up into 4 equal pieces. The bias field was adjusted within each piece to give a stairstep approximation of a non-uniform bias field. The segments had the same dimension in y as before (= 16mm) but each was only 4 mm wide in the x direction. Stated another way the ferrite block shown in Figure 3.7 was divided into to 4 equal segments with y directed cuts. For the two cases considered the data is presented in Figure 3.10. Case 1 in the plot is for a linear variation in the field strength from the left most segment to the right most. The field starts at 150 Oe and increases by 25 until it is 225 Oe in the last segment. Case 2 is a crude approximation to the field due to a small permanent magnet. The field in the center two segments is 200 Oe and in the outer two it is 150 Oe. As we can see for both cases the effect on the resulting radiation pattern is small.

Next we considered the antenna geometry described in Reference 17. In this case a small circular cross-section cylinder of ferrite was used as the substrate. The ferrite is approximately the same diameter as the circular patch that resides on top. The antenna is feed from below by a coax feed on one of the antennas edges. The dimensions of the geometry are given in Figure 3.11 (note we included in the model an iron block located above the patch where the biasing magnet was placed in the test setup). Regarding the ferrite characteristics we again had to make some educated guesses. For the ferrite characteristics we used: $4\pi M_s$=900 G, ΔH=2 Oe, ε_r = 14.3, internal bias = 150 Oe and the biasing field is z directed. The main effect being studied in [17] is the ability of a ferrite disk with a patch on top to generate a circularly polarized radiation field. The data we have from this model are shown in Figures 3.12 and 3.13. In the paper the measured circular polarization patterns for this antenna are presented. The values of the two polarization components were read off of the plot given in [17] an are include in the two

figures here. We included both of the main pattern cuts since the paper did not specify which cut plane they we using. As we can see we are able to accurately predict these patterns. To show how this antenna radiates a circular wave with only a single feed, a cut plane that cuts through the middle of the ferrite and is parallel to the x-y plane was used to study the antenna's operation. Figures 3.14 shows the shade plots of the electric field for several phase values. As we can see the energy from the feed couples to a wave on the puck and travels along the periphery of ferrite much the same as for a puck in a ferrite circulator. In this case though, the wave is radiating energy as it propagates.

Section 3.3 Conclusions

As we showed in this chapter the effect of surface and or volume waves on the radiation characteristics of a ferrite patch antenna is great. This limits the comparison of our simulations with data found using other analysis techniques. We were able to very accurately compute the radiated fields from a circular patch antenna on a finite ferrite substrate as shown in Figures 3.12 and 3.13. We were also able to show beam steer for a patch antenna on a finite ferrite substrate as shown in Figure 3.8. We were also able to show the surface wave present in larger substrates in Figures 3.4 and what was most interesting the coupling of energy to the surface of the ferrite in the case of the circularly polarized antenna in Figure 3.14.

The conclusion we can draw from this limited study is that using the bias field levels to steer a finite sized patch antenna seems to have limited usefulness. We do believe it can be a useful way to get a circularly polarized field with only a single feed point (saving a having to use two feeds and a phase shifter). We did note a recent paper from the literature where it is proposed that the variation of the bias field can be used to adjust the propagation constant of a signal on a microstrip feed network, and as such adjust the phase of the elements [14]. After the study we have to believe that this may be the most effective way to use ferrites in a scanning antenna array. We have not had the time yet to study the ideas presented in [14].

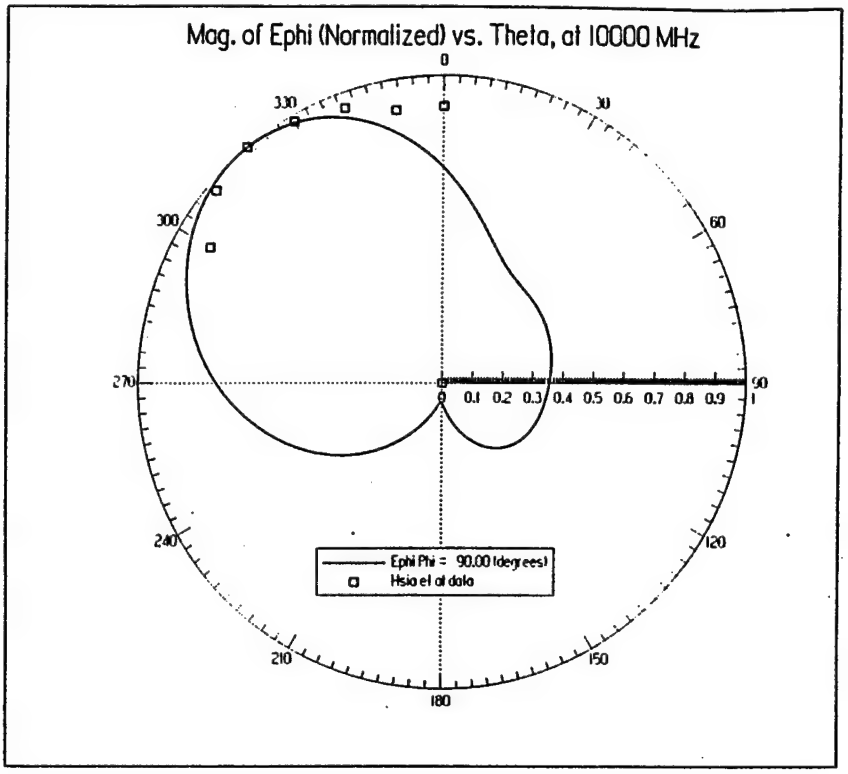

Figure 3.1 $|E_\phi|$ for current element on a grounded substrate with a biased ferrite superstrate.

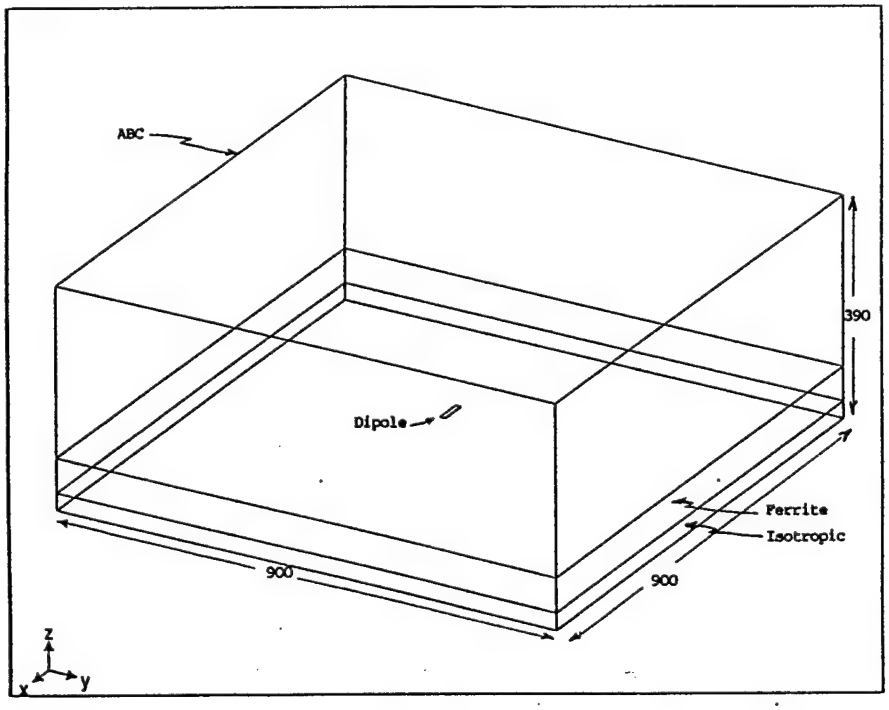

Figure 3.2 HFSS model of a current element on a grounded isotropic substrate with a biased ferrite superstrate. The isotropic layer is 30 mils thick and the ferrite is 60 mils thick. All D in mils.

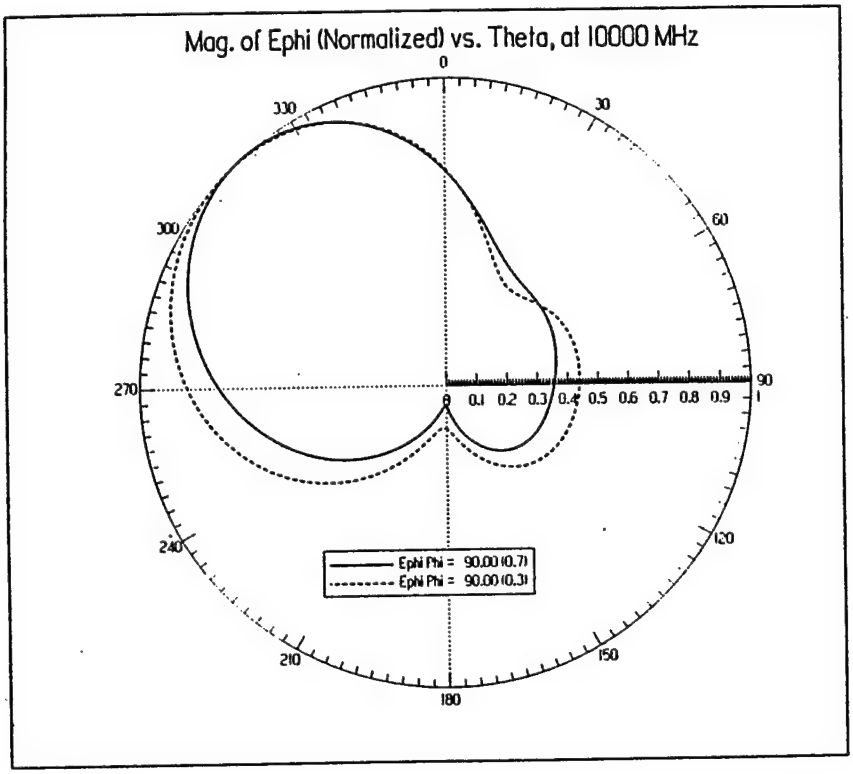

Figure 3.3 $|E_\phi|$ for model from Figure 3.2 for two different bias levels, $\omega_0 / \omega_m = 0.3$ and 0.7.

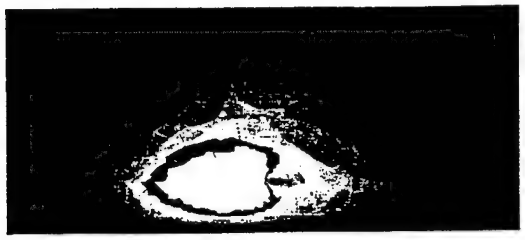

0

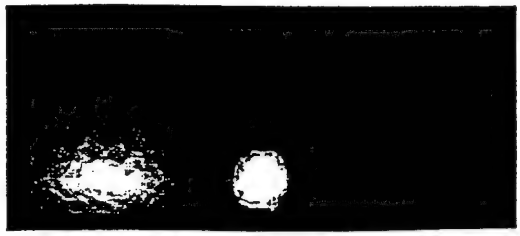

90

29

119

59

149

Figure 3.4 Shade plots of |E| for 6 different phase angles. The current element is the bright spot at the center. For the shading the maximum (brightest) is 5000 V/m and the darkest is 0 V/m. All phases in deg.

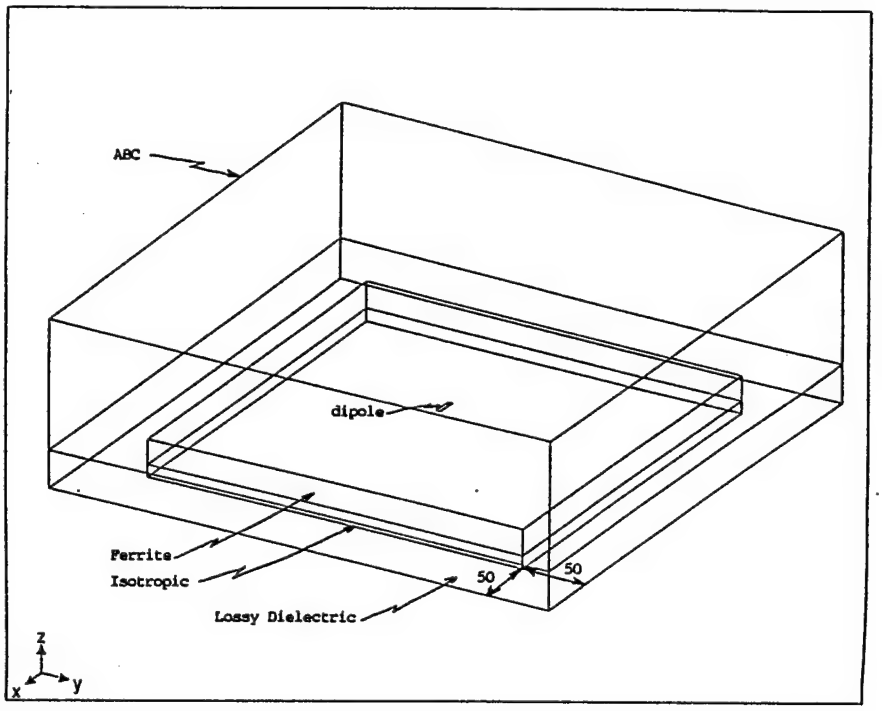

Figure 3.5 Revised model with lossy dielectric. All D in mils.

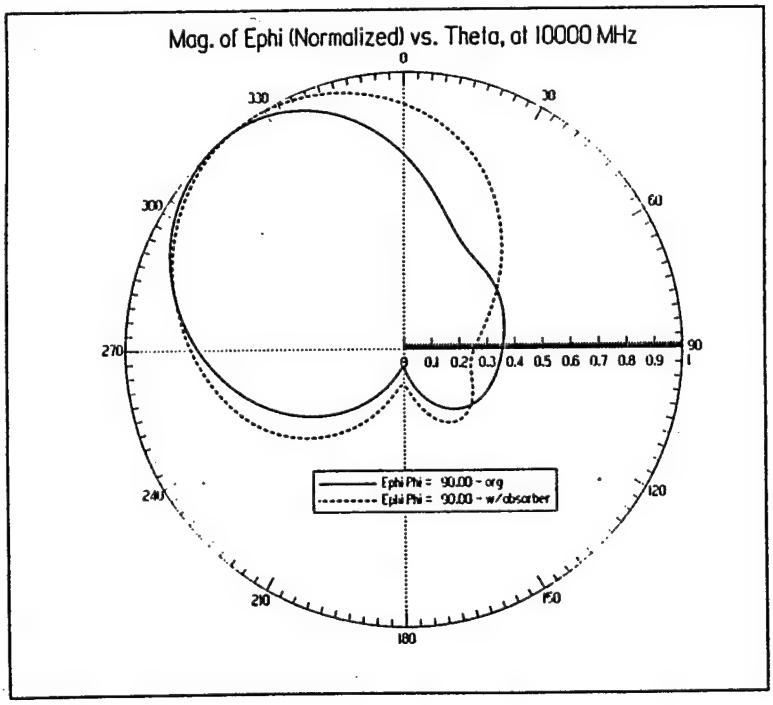

Figure 3.6 Comparisons of the computed $|E_\phi|$ for models from Figure 3.2 vs Figure 3.5.

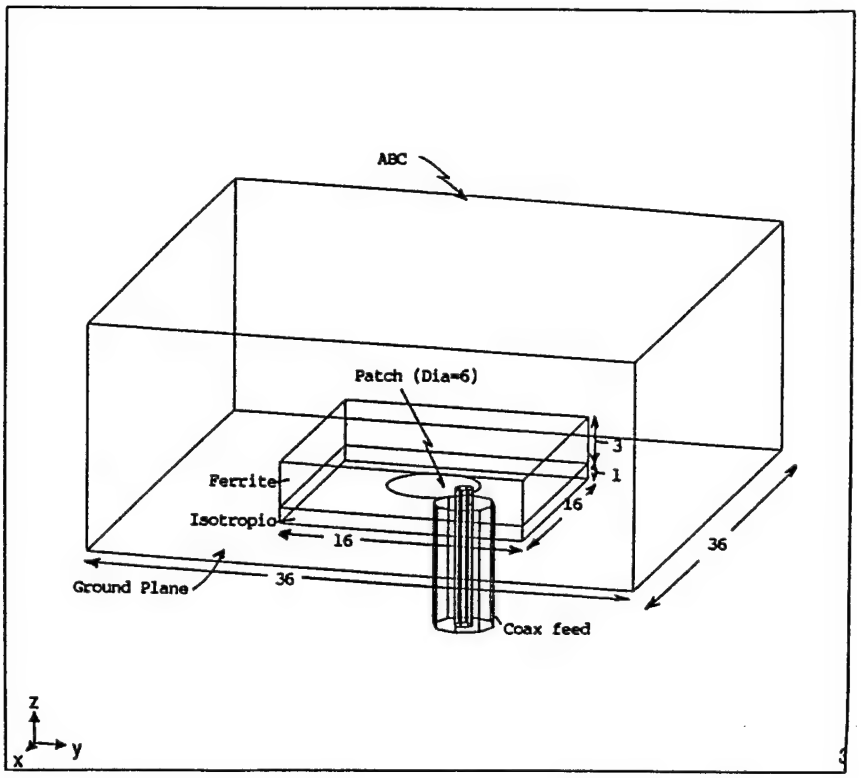

Figure 3.7 Circular patch antenna model with dimensions. All dimensions are in mm.

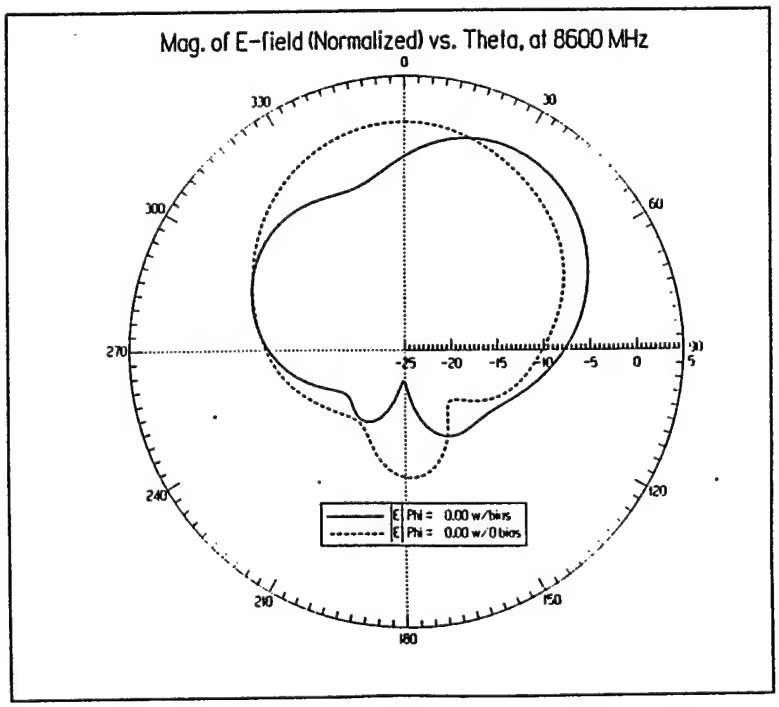

Figure 3.8 Far zone |E| for antenna from Figure 3.7 with and without a biasing magnetic field.

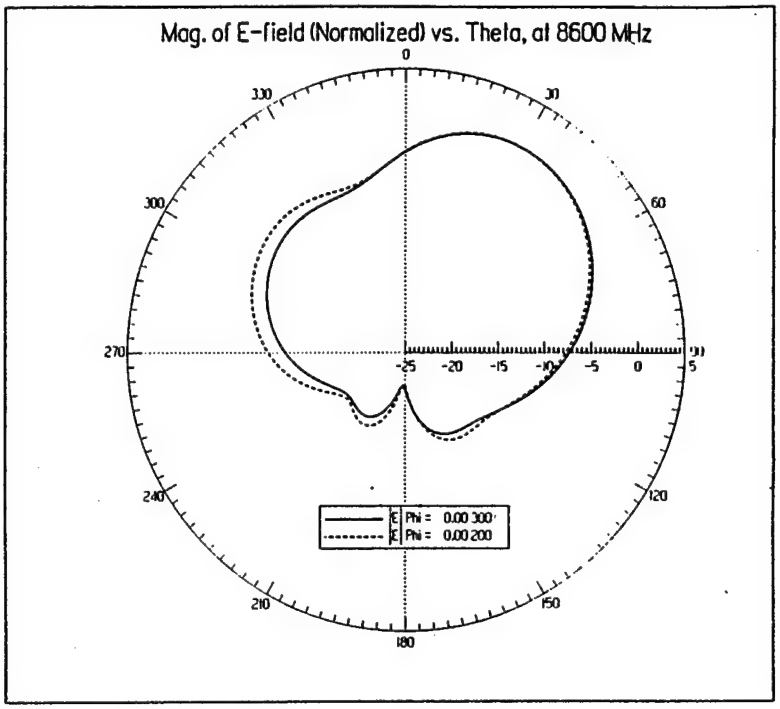

Figure 3.9 Comparison of far zone fields for 2 different bias field levels.

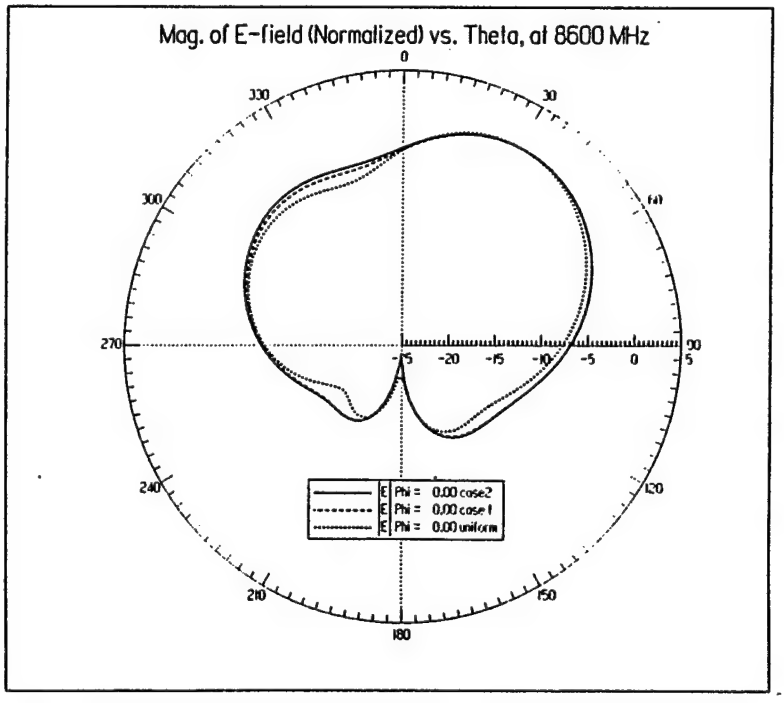

Figure 3.10 Far zone field plot for 3 different ferrites. Cases 1 and 2 have a non-uniform ferrite.

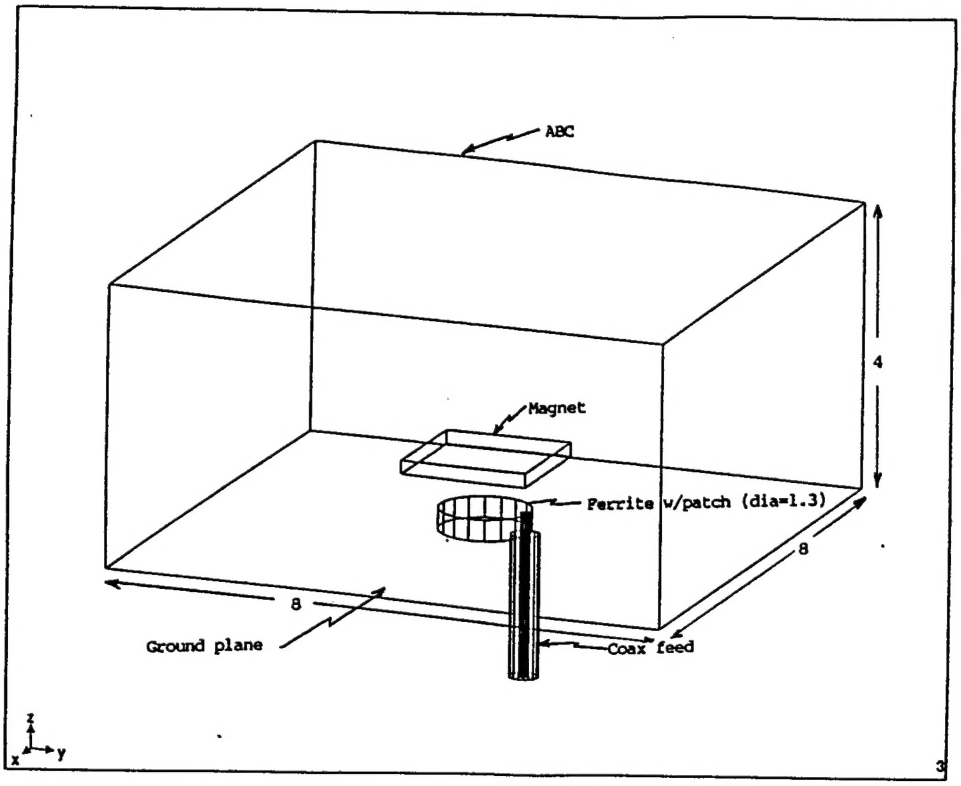

Figure 3.11 Circular patch antenna model. All dimensions are in cm.

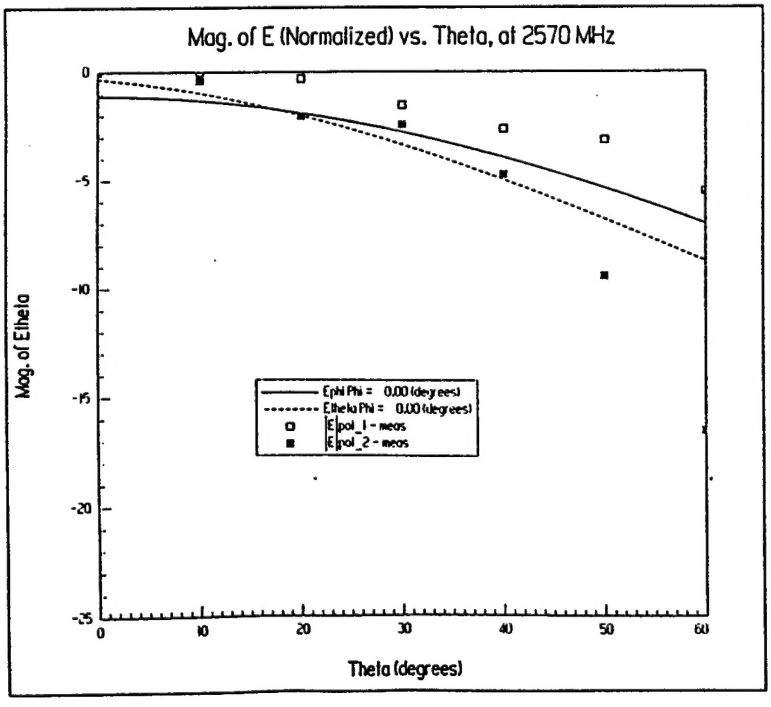

Figure 3.12 Far zone |E| for the two field components on a phi=0 deg. cut.

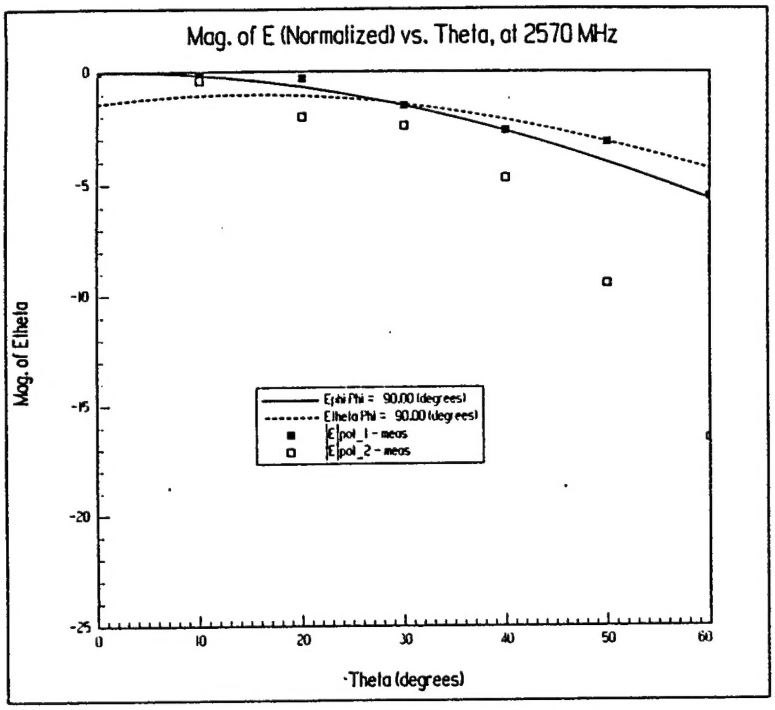

Figure 3.13 Far zone |E| for the two field components on a phi=90 deg. cut.

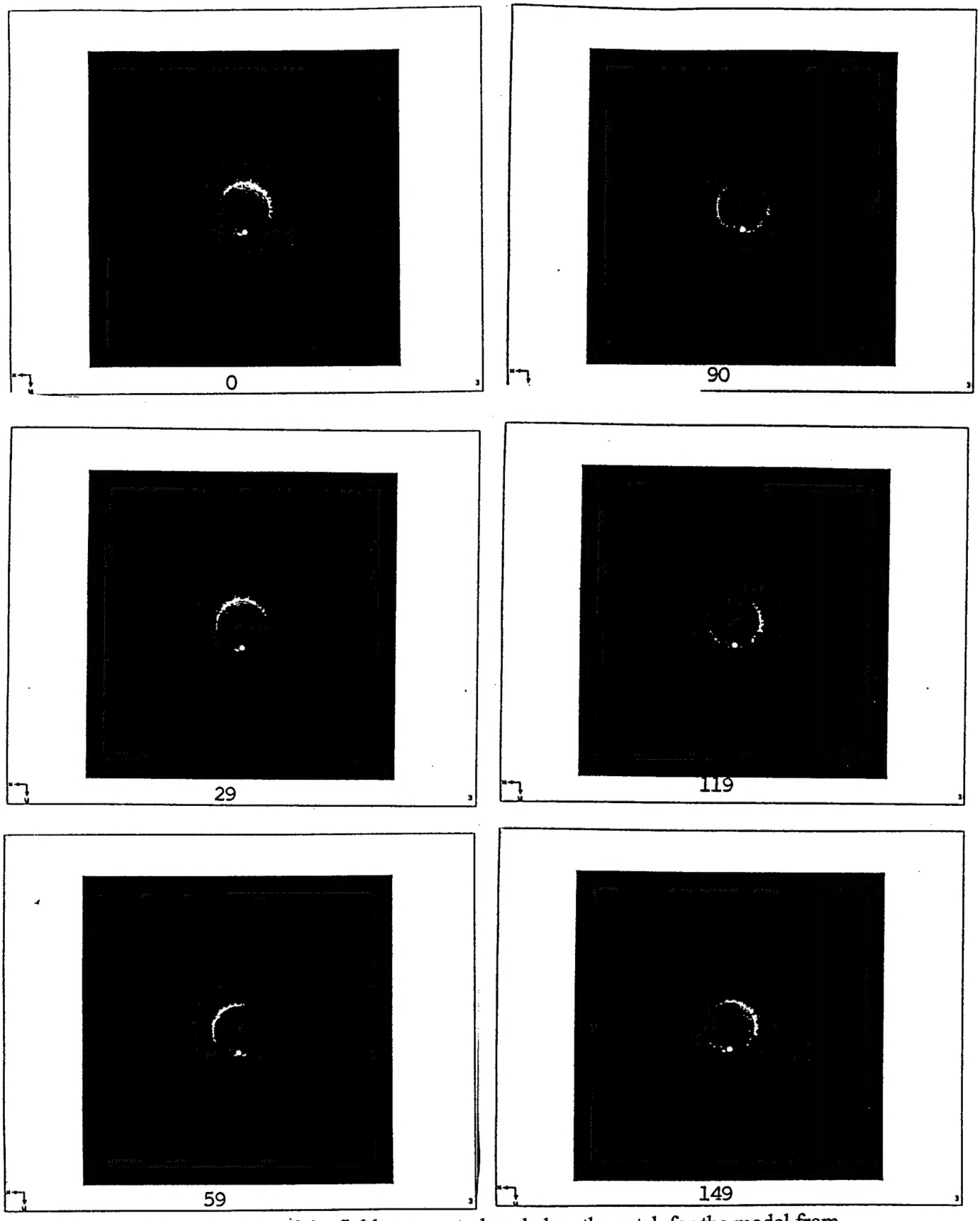

Figure 3.14 Shade plots of the fields on a cut plane below the patch for the model from Figure 3.11. The small white circle is the coax feed (the portion of the center conductor that passes through the substrate) and as the wave progresses around the puck you can see the outline of the ferrite. All phases in deg.

Chapter 4 Conclusion

We have seen from the data presented here that an FEM solver can be used to analyze ferrite patch antennas providing physical insight into the antenna's operation. This was most evident in the analyses shown in Figure 3.4 and 3.114 where we were able to "see" the surface wave being excited. As we stated in that chapter we believe that the discrepancy between our simulation data and that found using an infinite substrate Green's function is due to these surface waves. We were able to get reasonable results when simulating finite sized geometries.

Based on these results we see several areas for further work. First would be to analyze these surface waves and see exactly how they affect the device's performance. Second would be to use the matching boundary feature of HFSS once its complete to analyze an infinite array of patch antennas and to verify the results with those from Reference 15. Lastly, would be to use a solver such as this to investigate the array steering approach described in Reference 14.